

# Lawrence Berkeley National Laboratory

## LBL Publications

### Title

Theoretical Investigation of 2D Conductive Microporous Coordination Polymers as Li-S Battery Cathode with Ultrahigh Energy Density

### Permalink

<https://escholarship.org/uc/item/5sj744s5>

### Journal

Advanced Energy Materials, 8(25)

### ISSN

1614-6832

### Authors

Gao, Guoping  
Zheng, Fan  
Pan, Feng  
et al.

### Publication Date

2018-09-01

### DOI

10.1002/aenm.201801823

Peer reviewed

# Theoretical investigation of 2D Conductive microporous coordination polymers as Li-S battery cathode with ultrahigh energy density

Guoping Gao<sup>†</sup>, Fan Zheng<sup>†</sup>, Feng Pan<sup>§</sup>, Lin-Wang Wang<sup>†\*</sup>

<sup>†</sup>Materials Sciences Division, Lawrence Berkeley National Laboratory, Berkeley, California 94720, USA. E-mail: [lwang@lbl.gov](mailto:lwang@lbl.gov)

<sup>§</sup>School of Advanced Materials, Peking University, Shenzhen Graduate School, Shenzhen, 518055, People Republic of China

## Abstract

Even though tremendous achievement has been made experimentally in the performance of Li-S battery, theoretical studies in this area are lagging behind due to the complexity of the Li-S systems and effects of solvent. For this purpose, we have developed a new methodology for investigating the 2D hexaaminobenzene-based coordination polymers (2D-HAB-CP) as cathode candidate materials for Li-S battery via density functional theory calculation in combination with in-house developed charge polarized solvent model and genetic algorithm structure global search code. With high ratios of transition metal atoms and 2-coordinated nitrogen atoms, excellent electric conductivity, and structural porosity, the 2D-HAB-CP is able to address all of the three main challenges facing Li-S battery: confining the lithium polysulfides from dissolution, facilitating the electron conductivity and buffering the volumetric expansion during the lithiation process. In addition, the theoretical energy density of this system is as high as 1395 Wh/Kg. These results demonstrated that the 2D-HAB-CP is a promising cathode material for Li-S battery. Our proposed computational framework not only opens a new avenue in understanding the key role played by solution and liquid electrolytes in Li-S battery, but also can be generally applied to other processes with liquids involved.

## Introduction

Lithium-ion batteries (LIBs) are an integrated part of our daily life used in cell phone, laptop computers, and hybrid vehicle. The LIBs are composed of graphite anodes and Li transition-metal oxide (LTMO)/phosphate cathodes that intercalating Li ions with the minimal structural change due to the nature of intercalation and stabilities of the LTMO. However, the same factors also fundamentally limit its energy density<sup>[1]</sup>. The current LIB cathodes can reach an energy density of about 300 Wh/Kg, which is close to their theoretical limit<sup>[2]</sup>. The intercalation happens by Li donates its electron to the host while the transition metal atoms change their covalence states to accommodate the extra electron. Since this is more like the ionic interaction with no direct Li-transition metal bonding, the Li can often diffuse inside such LTMO. Nevertheless, non-covalent bonding also means weak binding strength and low energy density. To go beyond LIB, the community has worked on non-intercalation based battery<sup>2</sup>. The rechargeable lithium-sulfur (Li-S) battery is intensely studied for this purpose. Its theoretical energy density is 2567 Wh/Kg, which is 3-5 times higher than those of state-of-art LIBs<sup>[3]</sup>. In addition, sulfur

is cheap, earth-abundant, nontoxic, and environmental friendly element<sup>[4]</sup>. Unlike the LIBs, the Li-S battery works by the formation of chemical bonds between Li and S. Such bonds are weaker compared with Li-O bonds in the lithium air battery, hence it has smaller theoretical energy density than the lithium air battery<sup>[3, 5]</sup>, but at the same time, the Li-S reaction it is easier to manage and control compared to Li-O reaction. Thus, Li-S battery presents a compromise, which can serve as the first step to go beyond the LIBs. Given all these promises, there are however tremendous scientific and technical challenges which have hindered the commercialization of Li-S batteries<sup>[6]</sup>: (I) The shuttling effect stemming from the soluble lithium polysulfides ( $\text{Li}_2\text{S}_y$ ,  $4 \leq y \leq 8$ ), which causes the loss of active materials and rapid capacity fading. The intermediate lithiation states are completely soluble, and actually they can only sustain their voltages in the solvated states. This will cause the  $\text{Li}_2\text{S}_y$  to be decomposed on the Li metal anode and to lose capacity of the system; (II) the insulating nature of both sulfur and the final reduction product  $\text{Li}_2\text{S}$ , which impedes the lithiation process; (III) The 80% volumes change during cycling process, which causes structural damage and mechanical instability. One common method to address (II) and (III) is to use highly mesoporous conducting hosts to introduce electric conductivity and to buffer the volume change. For this purpose, the conductive porous carbon materials<sup>[7]</sup> are often used. However, the weak interaction between non-polar carbon and pure sulfur or  $\text{Li}_2\text{S}_y$  make it difficult to be used as an adhesive material to prevent Li-polysulfide dissolution (challenge I)<sup>[8]</sup>. To address this challenge, sometimes cage like electrodes are used to physically encapsulate S molecules and clusters<sup>[9]</sup>. However, such physical enclosure is difficult to realize and to be made stable<sup>[10]</sup>. Another possibility is to bind the  $\text{Li}_2\text{S}_y$  to a metal oxide substrate with strong adhesion<sup>[11]</sup>, so it will be prevented from dissolution thermodynamically. The key is to keep the high energy density despite the added weight of the substrate and the strong binding to the substrate. In this regard, the bulk substrate with small surface/volume ratio will be too heavy<sup>[11a]</sup>, thus 2D substrates or frameworks will be beneficial. Another advantage of using a 2D substrate is to provide electric conductivity<sup>[12]</sup>. On the other hand, transition metal can be used as an anchoring point for pure sulfur and  $\text{Li}_2\text{S}_y$ . For this regard, porous metal-organic framework (MOF) materials have been used<sup>[13]</sup>. Unfortunately, the MOF does not provide the necessary electric conductivity, thus some other electric binders must be added, which increase the complexity of the system<sup>[14]</sup>. What needed is a system, which is 2D, or 3D porous structure, contains transition metals and is also electrically conductive. Recently, a new class of material named 2D coordination polymer: 2D hexaaminobenzene-based coordination polymers (2D-HAB-CP), has been synthesized<sup>[15]</sup>. It consists of transition metal coordinately bonded with a small unit of conjugated polymer formed by C and N elements. Unlike the MOF, this system is electrically conductive, thus it satisfies the above criterions, combining the merits of both the porous carbon materials and MOFs as the Li-S battery cathode<sup>[15-16]</sup>. More excitingly, Bao et al have experimentally proved that the 2D-HAB-CP can exhibit high volumetric and areal capacitance as a Li-cathode material<sup>[17]</sup>. However, that work used the 2D-HAB-CP as it is, without the addition

of S. Thus it is not a sulfur battery, and the energy density is relatively low. In the present work, we will theoretically investigate the use of 2D-HAB-CP as a Li-S battery cathode by adding sulfur atoms on the substrate.

Even though tremendous achievement has been made experimentally in the performance of Li-S battery, theoretical studies in this area are lagging behind<sup>[18]</sup>. Part of the reason is the complexity of the Li-S systems. Unlike the LIBs, which happen in the crystal structure, the Li-S reactions have much more complex configurations. Direct first principle molecular dynamics simulation cannot be run long enough to directly simulate the reaction process. Thus, one has to search for the global minimum structures. The effects of solvent further complicate the issue<sup>[19]</sup>.  $\text{Li}^+$  is a highly polarizable ion, with strong ion-solvent interaction energy. Some of the commonly available solvent models diverge in this system. This makes it difficult even to study the energies of the isolated  $\text{Li}_2\text{S}_y$  molecule in the solvent. In this work, we developed an *ab initio* approach based on density functional theory (DFT) to study the Li-S battery energetics on 2D-HAB-CP substrate. At first, specific ion-solvent interaction parameters are developed for our continuum solvent model based on the experimental discharging voltage data for the  $\text{Li}_2\text{S}_y$  molecule in the electrolyte. Then the global minimum configurations are searched through an in-house developed genetic algorithm search code [Developed by Fan Zhen] for the structure of  $\text{Li}_2\text{S}_y$  on top of 2D-HAB-CP. The reaction energetics is analyzed based on the DFT calculations. We found that the transition metal atoms in 2D-HAB-CP can effectively capture the sulfur atoms, while the 2-coordinated nitrogen edges atoms are preferred sites for Li binding during the charge/discharge process. With sufficient Lithium, the system demonstrates a layer structure with alternating Li and S atoms, which resemble that of the bulk  $\text{Li}_2\text{S}$ . The highest energy density is about 1395 Wh/Kg. Besides, the 2D-HAB-CP can significantly reduce the dissolution of  $\text{Li}_2\text{S}_y$ , although it does not completely block it on the thermodynamic ground. Perhaps a changing of the transition metal like V or Cr, can further improve this aspect<sup>[6a, 20]</sup>. Finally, the system shows excellent electric conductivity throughout the lithiation process. As for the volumetric change of the system, we have introduced a 2D-HAB-CP/S/2D-HAB-CP sandwich structure. Preliminary tests show that its volume change during lithiation is as small as 3%, rivals that in LIB.

### Computation details

All calculations were performed using DFT coded in the PWmat code<sup>[21]</sup>. The exchange-correlation interactions were treated by the generalized gradient approximation<sup>[22]</sup> in the form of the Perdew - Burke - Ernzerhof functional<sup>[23]</sup>. The Van der Waals interaction was described by using the empirical correction in Grimme's scheme, i.e. DFT+D<sub>2</sub><sup>[24]</sup>. The spin=2 polarization was used in all the calculations. The electron wave-functions were expanded by plane waves with cut-off energies of 680 eV, and the convergence tolerance for residual force and energy on each atom during structure relaxation were set to 0.005 eV Å<sup>-1</sup> and 10<sup>-5</sup> eV, respectively. The vacuum space was more than 20 Å to avoid the interaction between periodical images. The Hubbard U (DFT+U) treatment was used on the transition metal. The U value for

Mn was set to 3.06 eV following the literature value<sup>[25]</sup>. The solvent effects were simulated with implicit charge polarizable solvent model<sup>[26]</sup>, which uses fixed ion charge to define the onsite of the dielectric function. We found that the self-consistent continuum solvation model (SCCS) model<sup>[27]</sup> was difficult to converge for the case of Li. The solvent dielectric constant used in the solvent model is fit to be 7.8 to simulate the solvent effects of DME/DOL (1: 1, v: v). The choice of other solvent model parameters will be discussed later. The model is efficient to include approximate solvent effects where the solvent is not an active constituent in the reaction or process<sup>[28]</sup>. So, no explicit solvent molecules are present in our calculation. For crystal calculations, the solvent model should not be used. More details of free energy calculation can be found in the supporting information (SI).

## Results

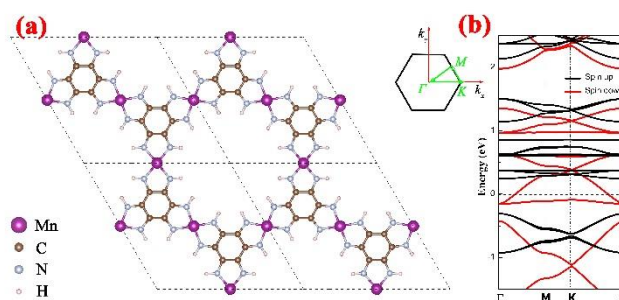


Figure 1(a) The geometric structure of Mn-HAB-CP monolayer. (b) The band structure of Mn-HAB-CP monolayer along the high symmetry  $\Gamma$ -K-M- $\Gamma$  directions and the associated Brillouin zone. The Fermi energy in the band structure is at 0.

Figure 1a presents the configuration of the 2D-HAB-CP, which has been synthesized using the “bottom-up” method<sup>[15]</sup>. It is structurally stable against phonon vibrations. The unit cell of 2D HAB-CP consists of three equivalent transition metal (TM) atoms (linkers) in a hexagonal honeycomb lattice. Each TM atom is surrounded by four N atoms forming a square planar arrangement of nitrogen-coordinated metal macrocycles. Based on our initial calculation, the interaction between  $S_8$  and transition metal will weaken with the number of  $d$ -electrons and the late transition metals, such as Zn, cannot capture the  $S_8$  firmly which is confirmed by previous work as well<sup>[29]</sup>. On the other side, the 2D hexaaminobenzene-based coordination polymers with early transition metal, like Sc or Ti, cannot maintain metallic nature due to the lack of spare  $d$ -electrons for  $d$ - $p$ - $\pi$  conjugation. Therefore, Mn is chosen as the compromise TM linker to investigate the potential of Mn-HAB-CP in the Li-S batter application. The metallic nature of Mn-HAB-CP, due to the effects of  $d$ - $p$ - $\pi$  conjugation, is confirmed by the no-gap band structure shown in Fig. 1b. The band structure has a relatively large dispersion at the Fermi energy, which indicates band-like charge transport, instead of localized state hopping.

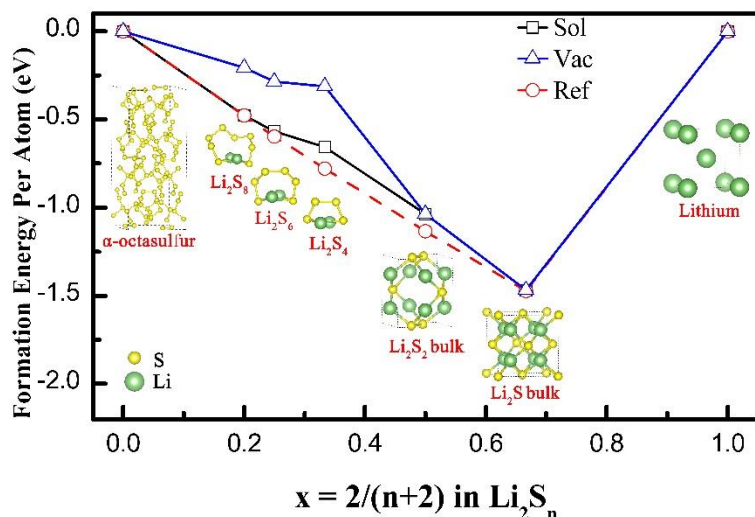


Figure 2 The computational Gibbs free formation energies of some key polysulfide per atom involved in different lithiation stages in the vacuum (black line) and DME/DOL (v:v, 1:1) electrolyte (blue line). The experimental formation energies converted from the experimental charging/discharging voltages are present in the red dash line as a reference.

Before the calculation of Li polysulfides binding with the substrate, it is necessary to first study the Gibbs free formation energy of the  $\text{Li}_2\text{S}_y$  molecules in the electrolyte. In the experiment, the Li-S battery operator in the electrolyte solvents, such as 1,2-dimethoxyethane (DME) or 1,3-dioxolane (DOL). One of the problems of Li-S battery, the shuttle effect, is caused by the dissolution of lithium polysulfide ( $\text{Li}_2\text{S}_y$ ,  $4 \leq y \leq 8$ ) in the solvent. However, it is a long-standing challenge to theoretically predict the solvent behaviors of polysulfide and to calculate the solvated Gibbs formation energies of these polysulfide<sup>[19, 30]</sup>. In our calculation, the charge polarizable solvent model with a fixed ion charge to determine the dielectric function profile, is used to represent the solvent effect. Nevertheless, the onsite distance of the dielectric screening from the Li nuclear is a critical parameter which determines the solvation energy. Unfortunately, at this stage, direct *ab initio* calculation with the default parameter for the solvation model does not provide accurate solvation energy. To solve this problem, we have used experimental results to fix our solvent model parameter. Experimentally, the charging/discharging voltages for the stage from  $\text{S}_8$  to  $\text{Li}_2\text{S}_4$  are known. Since the  $\text{Li}_2\text{S}_y$  ( $4 \leq y \leq 8$ ) are dissolved in the solvent as molecules, these charging voltages effectively provide the Gibbs free formation energies of these molecules in the electrolyte (The conversion method between calculated Gibbs free formation energies and experimental voltage can be found in section 2 of the supporting information (SI)). We can thus adjust our solvent model parameter to reproduce the experimental curve<sup>[31]</sup>. Note that, the states of Li,  $\text{Li}_2\text{S}$ ,  $\text{Li}_2\text{S}_2$ , and  $\text{S}_8$  are all in solid crystal form, thus there is no solvent effect. As a fit, we have chosen an ion-charge induced dielectric profile parameter of 7.8 in the PWmat implementation in order for our solvent model to agree with the experiment as shown in Fig. 2. The induced

polarization charges of  $\text{Li}_2\text{S}_y$  ( $4 \leq y \leq 8$ ) are shown in Figure S1 of the SI. The experimental formation energies converted from the experimental charging/discharging voltages<sup>[4b, 31]</sup> are shown in Figure 2 as the dashed line. We find that the experimental formation energy of final production (bulk  $\text{Li}_2\text{S}$ ,  $-1.47$  eV per atom) can be obtained by the most stable  $\alpha$ -octasulfur, and Li crystal structures<sup>5</sup> [ $\frac{1}{8}\text{S}_8(\text{s}) + \text{Li}(\text{s}) \rightarrow \text{Li}_2\text{S}(\text{s})$ ]. There are some debates for the existence of  $\text{Li}_2\text{S}_2$  and its structure in the solvent<sup>[32]</sup>. Using the fitted solvent model parameter, the formation energy of one  $\text{Li}_2\text{S}_2$  molecule in the solvent is only  $-0.74$  eV per atom, far higher from the experimental value ( $-1.14$  eV per atom). We also find that, no matter what parameter we use, we cannot obtain a good fit of  $\text{Li}_2\text{S}_2$  energy to the experiment if it exists as a dissolved molecule. On the other hand, if the bulk crystal structure as predicted by Yang et al<sup>[33]</sup> is used for  $\text{Li}_2\text{S}_2$ , the formation energy will be  $-1.04$  eV per atom [ $\frac{1}{4}\text{S}_8(\text{s}) + \text{Li}(\text{s}) \rightarrow \text{Li}_2\text{S}_2(\text{s})$ ], which is close to the experimental value. This can be viewed as a peripheral proof the  $\text{Li}_2\text{S}_2$  should exist as a crystal or large cluster in the solvent, consistent with the conclusion of a recent molecular dynamics simulation<sup>[32b, 34]</sup>. For  $\text{Li}_2\text{S}_4$ ,  $\text{Li}_2\text{S}_6$  and  $\text{Li}_2\text{S}_8$  clusters [ $\frac{y}{8}\text{S}_8(\text{s}) + \text{Li}(\text{s}) \rightarrow \text{Li}_2\text{S}_y(\text{aq}), 4 \leq y \leq 8$ ], the formation energy in the vacuum can be higher than that of the experimental values by  $0.5$  eV per atom indicating the importance of the solvation energy. After including the solvent effects, the biggest difference between the theoretically predicted formation energy and the experiment is about  $0.1$  eV per atom. The overall agreement between experiment and theory is good, in line with the general accuracy of the DFT calculations.

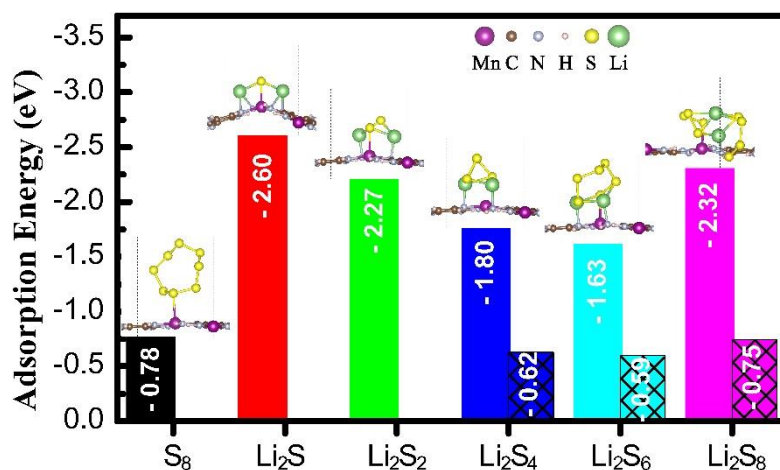


Figure 3 The adsorption energy of isolated  $\text{S}_8$ , and  $\text{Li}_2\text{S}_y$  molecule on Mn-HAB-CP in the vacuum (bars without pattern) and solvent (bars with net pattern).

Having fixed the solvent model, we can now estimate the binding of  $\text{Li}_2\text{S}_y$  ( $4 \leq y \leq 8$ ) to the Mn-HAB-CP in the solvent. We have calculated the  $\text{Li}_2\text{S}$ ,  $\text{Li}_2\text{S}_2$  and  $\text{S}_8$  binding on Mn-HAB-CP in the vacuum environment, while  $\text{Li}_2\text{S}_y$  ( $4 \leq y \leq 8$ ) in both solvent and vacuum environments (Figure 3). The  $\text{S}_8$  molecule binds on top of one Mn atom with

an adsorption energy of  $-0.78$  eV, indicating that it can be absorbed and melt on the Mn-HAB-CP substrate due to the existence of the transition metal. It was found that, in pure carbon nitride 2D systems, the  $S_8$  will not bind to the substrate<sup>[32a]</sup>. For  $Li_2S$ , the S atom is bind on the Mn site, while each Li atom is grasped firmly by two nitrogen atom. The adsorption energy of  $Li_2S$  molecular on Mn-HAB-CP is as high as  $-2.60$  eV, which is  $-1.46$  eV stronger than it on graphene (Fig S2 in SI) and comparable with that on two-dimensional transition metal disulfides<sup>[35]</sup>. The other polysulfides also show similar adsorption behavior on Mn-HAB-CP and exhibit strong binding strength. The adsorption energies of  $Li_2S_4$ ,  $Li_2S_6$ , and  $Li_2S_8$  are  $-1.80$  eV,  $1.63$  eV and  $-2.32$  eV respectively when measured in vacuum. In the solvent, the bonding distance of polysulfides from the Mn and N anchoring atoms increase slightly and the adsorption energies reduce to  $-0.62$  eV,  $-0.59$  eV and  $-0.75$  eV for  $Li_2S_4$ ,  $Li_2S_6$ , and  $Li_2S_8$ , respectively. These negative adsorption energy values indicate that the polysulfides prefer to be adsorbed on the Mn-HAB-CP rather than being extricated in the solvent. Therefore, the high ratios of both Mn and N atoms in Mn-HAB-CP enable it as a bi-functional host for lithium polysulfide, which not only captures and but also electrically activates the insolating  $S_8$ .



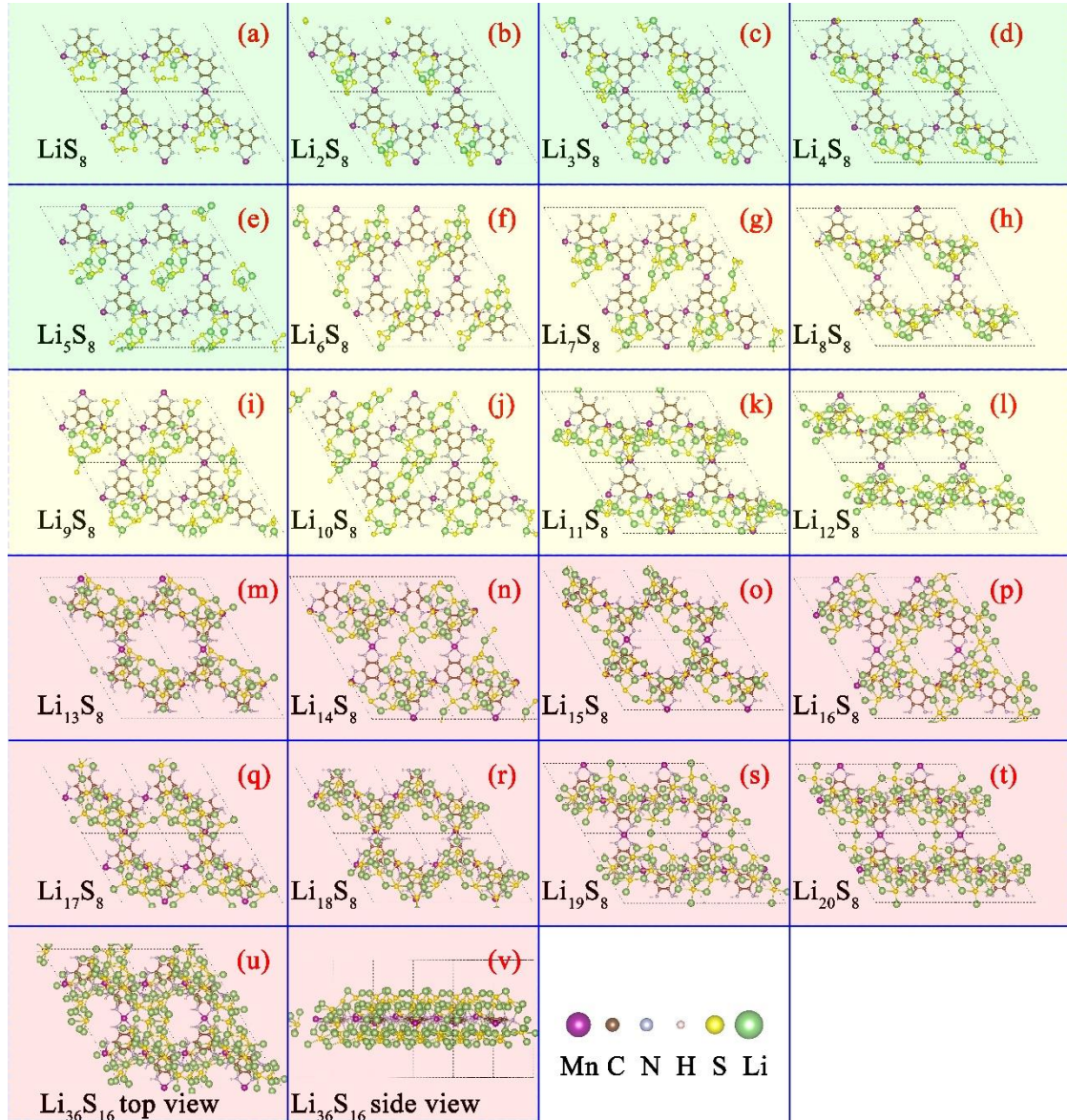


Figure 4 The optimized stable structure of  $\text{Li}_x\text{S}_8$  adsorbed on Mn-HAB-CP obtained via genetic algorithm global search. The side views of these structures are shown in Figure S3 in supporting information. The isolated, linear, and meshed  $\text{Li}_x\text{S}_8$  are distinguished by green, yellow and red background color, respectively.

To further study the lithiation process, we first place one  $\text{S}_8$  molecular per unit cell on Mn-HAB-CP, then gradually add Li atoms to the cluster to form  $\text{Li}_x\text{S}_8$  until twenty lithium atoms have been added. The global energy minimum structures of  $\text{Li}_x\text{S}_8$  binding to the two-dimensional coordination polymers are obtained using our in-house code, which implements the genetic algorithm to find the global minimum<sup>[36]</sup>. For each generation, the DFT relaxation of the populations is performed with PWmat. The process of our global minimum structure search code is present as the Fig. S3 in supporting information. The global energy minimum configurations are shown in Figure 4 (a-t). In the beginning, when there is no Li atom, the  $\text{S}_8$  is attached to the Mn as shown in Fig. 3. The first lithium atom opens the  $\text{S}_8$  ring with one S atom binding

on a Mn atom and the Li atom binding on a nitrogen atom ( $\text{LiS}_8$ , see Fig. 4a). With the second lithium added, the  $\text{Li}_2\text{S}_8$  cluster is in a dumbbell shape with two  $\text{S}_4$  isomers at each end. The third added lithium will bridge between the end of one  $\text{S}_4$  isomer of  $\text{Li}_2\text{S}_8$  and two nitrogen atoms of Mn-HAB-CP ( $\text{Li}_3\text{S}_8$ , see Fig. 4c). In the  $\text{Li}_4\text{S}_8$  and  $\text{Li}_5\text{S}_8$ , the  $\text{S}_4$  isomers are divided by lithium atoms into smaller ones, like  $\text{S}_2$ , and  $\text{S}_3$ . With more than six lithium atoms,  $\text{Li}_x\text{S}_8$  ( $6 \leq x \leq 11$ ) forms parallel one-dimensional wires. The S isomers larger than  $\text{S}_2$  disappear. When the lithium number is larger than 11, the one-dimensional  $\text{Li}_x\text{S}_8$  wires interweave into a two-dimensional three-layers-sandwich like structure: two lithium layers and one sulfur layer. The  $\text{S}_2$  dimmers observed in earlier structures are melting into isolated S atoms gradually forming the middle layer of the sandwich framework with two layers of lithium atoms exposed (see Fig. S5 in supporting information). One lithium layer attaches to the Mn-HAB-CP firmly, and there is no Mn-S binding remaining.

The above configurations only consider  $\text{Li}_x\text{S}_8$  at one side of Mn-HAB-CP. In reality, both sides can attach  $\text{Li}_x\text{S}_8$  simultaneously. To study that, we have added another  $\text{Li}_{16}\text{S}_8$  cluster on the other side of the Mn-HAB-CP- $\text{Li}_{20}\text{S}_8$  structure to fully explore the Li-S battery potential. This  $\text{Li}_{16}\text{S}_8$  cluster forms another two-dimensional sandwich framework on the other side of Mn-HAB-CP (see Fig. 4 (u) and (v)). We do find that, if  $\text{Li}_{20}\text{S}_8$  is added to the other side of Mn-HAB-CP- $\text{Li}_{20}\text{S}_8$ , the structure becomes unstable.

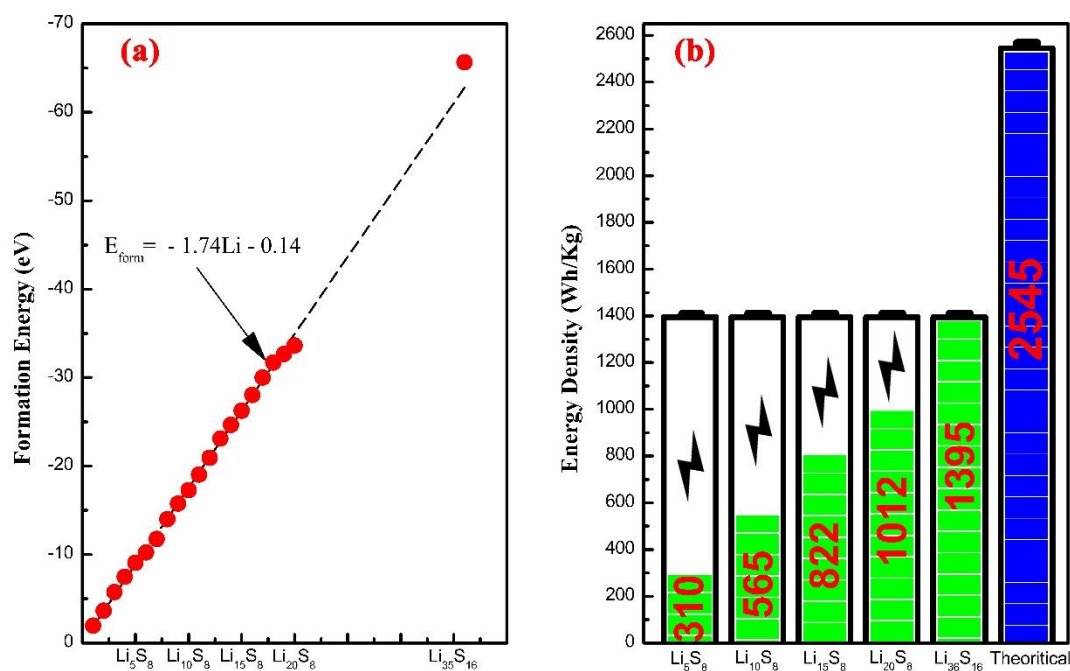


Figure 5, (a) the overall formation energy of  $\text{Li}_x\text{S}_y$  on Mn-HAB-CP as a function of the number of Li in the solvent ( in red color). The fit equations are plotted in black dash-dot lines. (b) The energy density of  $\text{Li}_x\text{S}_y$  on the Mn-HAB-CP with solvent effects at different lithiation stages.

Figure 5a plots the formation energy of  $\text{Li}_x\text{S}_y$  on Mn-HAB-CP as a function of the number of Li in the solvent. The formation energy is calculated as following:

$$E_{form} = E_{Li_xS_8 \text{ on Mn-HAB-CP}} - E_{S_8-Mn-HAB-CP} - xE_{Li \text{ bulk per atom}} \quad (1)$$

Here,  $E_{Li_xS_8 \text{ on Mn-HAB-CP}}$ , and  $E_{S_8-Mn-HAB-CP}$  are the total energy of  $Li_xS_y$  on Mn-HAB-CP, and  $S_8$  on Mn-HAB-CP calculated in solvent, respectively.  $E_{Li \text{ bulk per atom}}$  is the energy per Li atom in its bulk form. Remarkable, the formation energy of  $Li_xS_8$  is almost a linear line of the number of Li. The linear formation energy as a function of the lithium atom indicates a constant voltage (1.74 Volt) during the charge and discharge process, a very good feature and a significant advantage compared to other cathode materials for battery design. This linear behavior only bends a little when the number of Lithium atom increases to 19, and 20. The overall the total formation energy of  $Li_{20}S_8$  on Mn-HAB-CP in the solvent is -33.65 eV. This value reaches to -65.67 eV when we add another  $Li_{16}S_8$  cluster on the other side of Mn-HAB-CP. The energy density of  $Li_xS_y$  on the Mn-HAB-CP with solvent effects at different lithiation stages are shown in the Fig. 5b. The energy density is 310 Wh/Kg with only five lithium added ( $Li_5S_8$ ). With 10 lithium added, the energy density is 565 Wh/Kg, which is comparable with the state-of-the-art Li-S value obtained in experiment<sup>[37]</sup>. The energy density increase to 1012 Wh/Kg when only one side of the Mn-HAB-CP is fully loaded with  $Li_{20}S_8$ , and the value further reach 1395 Wh/Kg if both side are fully loaded (Mn-HAB-CP- $Li_{36}S_{16}$ ).

Table 1 The separation energies of Mn-HAB-CP- $Li_xS_y$  into dissolved  $Li_2S_y$  and the remaining Mn-HAB-CP bounded cluster. The total energies of Mn-HAB-CP- $Li_{10}S_8$  and Mn-HAB-CP- $Li_{20}S_8$  are set to be zero.

$Li_{10}S_8$	$Li_9S_4+1/2Li_2S_8$	$Li_9S_5+1/2Li_2S_6$	$Li_9S_6+1/2Li_2S_4$
0	0.59	-0.23	-0.49
$Li_{20}S_8$	$Li_{19}S_4+1/2Li_2S_8$	$Li_{19}S_5+1/2Li_2S_6$	$Li_{19}S_6+1/2Li_2S_4$
0	13.86	10.31	6.24

We next study the ability of the system to prevent the dissolution of Li-polysulfide. As shown in Fig. 1b, the binding energy of the  $Li_2S_y$  and Mn-HAB-CP are all negative in the solvent, which means the Mn-HAB-CP itself can absorb the isolated  $Li_2S_y$  in the solvent. However, if we propose to use Mn-HAB-CP- $S_8$  or Mn-HAB-CP- $2S_8$  as the starting electrode and gradually lithiate the system, a more relevant question is whether some  $Li_2S_y$  cluster can be separated from the Mn-HAB-CP- $Li_xS_8$  or Mn-HAB-CP- $Li_x2S_8$  system and to be dissolved in the solvent. Due to the large number of possible systems and configurations, we have used the Mn-HAB-CP- $Li_{10}S_8$  and Mn-HAB-CP- $Li_{20}S_8$  as two presentative systems to study the dissolution stability. Some of the results are shown in Table I. Here we have focused on  $Li_2S_8$ ,  $Li_2S_6$  and  $Li_2S_4$  molecules since they can be dissolved in the solvent. We see that, for 1/2  $Li_2S_6$  and 1/2  $Li_2S_4$  from Mn-HAB-CP- $Li_{10}S_8$  unit, the dissolution energy is slightly negative, -0.23 eV and -0.49 eV indicating that Mn-HAB-CP- $Li_{10}S_8$  is thermodynamically unstable against the dissolution. On the other hand, the dissolution energy is positive for all the other cases. In particular, the

dissolution energy is extremely large for the case of one  $\text{Li}_2\text{S}_8$  molecule separated from two Mn-HAB-CP  $-\text{Li}_{20}\text{S}_8$ . This is because what left behind Mn-HAB-CP  $-\text{Li}_{19}\text{S}_4$  is a rather high energy structure with too many lithium atoms but a small number of S atoms. We do caution that the dissolution can be a complicated process with many more possible configurations than the one considered here. Future more detailed and comprehensive studies are necessary. For the small negative dissolution energy cases, we also note that such energy is much smaller than the original Li-S battery, where the  $\text{Li}_2\text{S}_y$  cluster for ( $4 \leq y \leq 8$ ) has to be dissolved into the solvent in order for the lithiation process to continue. In another word, the dissolved state is one step in its lithiation process, and the dissolution is necessary in order to reach the final reduction result (and it also serves as a way to conduct the electric current). In our case, the situation is different. Even though thermodynamically it is not stable against the dissolution in the early stage of the lithiation, it is stable in the later stage of the lithiation, and in order to carry out the discharge at a constant voltage, the intermediate states do not need to be dissolved. This means the kinetic process might be very different from the original Li-S design. Nevertheless, this is an important question worth further study in the future. Other improvements might be possible to enhance the stability, for example, using other transition metal, e.g. V, to replace Mn to have a larger binding energy with S. Perhaps longtime molecular dynamics simulation can also be used to directly monitor the behavior of discharging process.

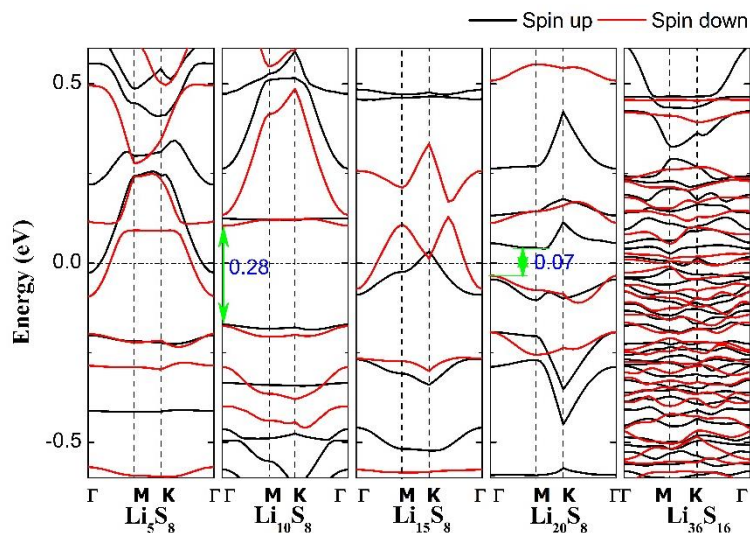


Figure 6 The band structures of Mn-HAB-CP with  $\text{Li}_x\text{S}_y$  clusters along the high symmetry  $\Gamma$ -K-M- $\Gamma$  directions in the solvent. The associated Brillouin zone is shown in the figure 1. The Fermi energy in the band structure is at 0.

As discussed in the introduction, conductivity is another critical issue for a good cathode in Li-S battery. We have shown in Fig. 1b that pristine Mn-HAB-CP is metallic in the vacuum. The electronic properties can change in solution or after it absorbs Li-S clusters. The Fig. 6 presents the band structure of various

Mn-HAB-CP-Li<sub>x</sub>S<sub>y</sub> in the solvent. With Li<sub>5</sub>S<sub>8</sub> on the Mn-HAB-CP, the system is metallic. When Li<sub>10</sub>S<sub>8</sub> is absorbed on Mn-HAB-CP, a small band gap of 0.28 eV is open up. This small gap is closed slowly as the lithium number increase. In case of Li<sub>20</sub>S<sub>8</sub>, the band gap is only 0.07 eV. In addition, with Li<sub>x</sub>S<sub>y</sub> clusters loading on both side of Mn-HAB-CP (Li<sub>36</sub>S<sub>16</sub>), the system is metallic. In the real experimental situation, the Li-S clusters will be loaded on both sides of Mn-HAB-CP simultaneously. We expect the system is always metallic, or very close to metal.

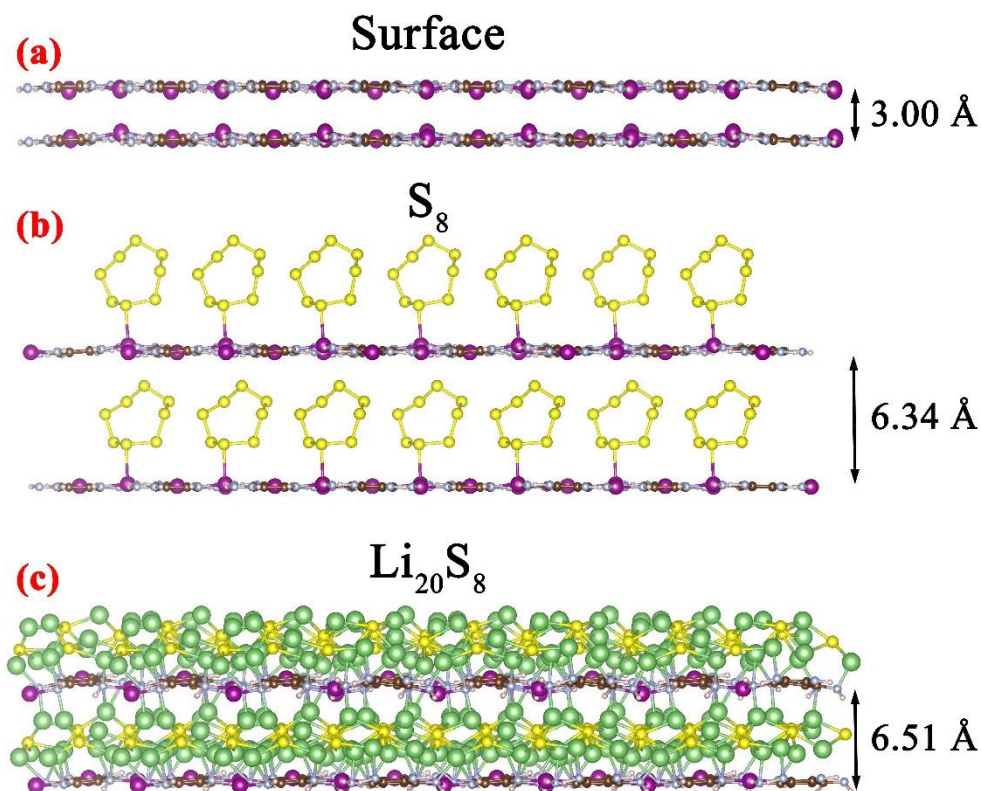


Figure 7 The interlayer distance of two layers of Mn-HAB-CP (a), S<sub>8</sub> loaded Mn-HAB-CP (b), and Li<sub>20</sub>S<sub>8</sub> loaded Mn-HAB-CP (half charged, c), The color codes of elements refer to Fig. 4.

In above, we have addressed two of the three challenges facing Li-S battery, the dissolution of Li-polysulfide, and the insulating nature of the cathode material. Another challenge is the volume expansion. So far, we have only studied systems with Li-S absorbed on the two sides of Mn-HAB-CP. The system is essential 2D. If the system is always 2D, its volumetric capacity will be rather small. One approach to solve this problem is to construct a 3D porous system, or mix Mn-HAB-CP 2D flakes with other conductive binders like carbon black. Here, we briefly introduce a design which sandwiches the Li-S layer with two layers of Mn-HAB-CP. As a matter of fact, it can be stacked up into a periodic 3D system with artificial layer structure. Such a design not only can increase the volumetric capacity, and it also has a potential to prevent the dissolution problem discussed above. While a full exploration of such a system deserves a separated detailed study, especially for the ability to diffuse the Li

into such a 3D structure, here we like to focus on one interesting issue: the volume expansion of the system upon lithiation. As shown in Fig. 7, In the starting electrode Mn-HAB-CP-S<sub>8</sub>, the Mn-HAB-CP/ Mn-HAB-CP interlayer distance is 6.34 Å (see Fig. 7b). However, when 20 lithium atoms are added to each Mn-HAB-CP-S<sub>8</sub>, making it Mn-HAB-CP-Li<sub>20</sub>S<sub>8</sub>, the Mn-HAB-CP/ Mn-HAB-CP distance only increases to 6.51 Å. Thus, there is only 2.7% lattice constant increases in the z-direction. This is rather remarkable, and the distance increase is similar to that of the LIB battery.

## Conclusion

The 2D hexaaminobenzene-based coordination polymers have been investigated as Li-S battery cathode via DFT calculation in combination with in-house developed charge polarized solvent model and genetic algorithm global structure search algorithm. The parameters of the solvent model are fixed by comparing the Li<sub>2</sub>S<sub>y</sub> (for y=4,6,8) molecule energies in the solvent with the experimental charging/discharging voltages. For a given chemical formula compound, the genetic algorithm is used to find the minimum energy configuration. Through our theoretical studies, we have the following conclusions: (1) The pristine Mn-HAB-CP will absorb Li<sub>2</sub>S<sub>y</sub> molecules from the solvent, and the transition metal will also absorb S<sub>8</sub> molecule to its surface to be bonded with the Mn atom; (2) With more lithium atoms added to the Mn-HAB-CP-S<sub>8</sub> or Mn-HAB-CP-2S<sub>8</sub> system, the S<sub>8</sub> will be broken into smaller and smaller pieces. Different structure patterns will be formed, from parallel wires eventually to Li-S alternating layer structures resemble that in crystal Li<sub>2</sub>S. In the fully lithiated structures, there is no more Mn-S bond, instead, Li layer will be first bound with the Mn-HAB-CP, followed by the S layer. Li atoms are bonded with the 2-coordinated edge N atoms; (3) The lithiation formation energy is almost a straight line of the number of Li atoms, indicating a constant voltage of about 1.74 V for the whole charge/discharge process. The final energy density for the Mn-HAB-CP-Li<sub>20</sub>S<sub>8</sub>-Li<sub>16</sub>S<sub>8</sub> final product is 1395 Wh/Kg; (4) While for the final product Mn-HAB-CP-Li<sub>20</sub>S<sub>8</sub>, the system is thermodynamically stable against dissolution/separation of Li<sub>2</sub>S<sub>y</sub> (y=4,6,8) molecules, the system could be thermodynamically unstable at the intermediate stage as for Mn-HAB-CP-Li<sub>10</sub>S<sub>8</sub>. Further studies are needed to address this issue, especially for the kinetic path of the molecule dissolution, or to find ways to increase the S-substrate binding energy; (5) The electrode is metallic throughout the charging/discharge process, hence solving the insulating problem in the original Li-S battery set-up; (6) A sandwiched design is proposed, which changes the 2D electrode into a 3D system, hence provides sufficient volumetric capacity. It is found that the vertical expansion of the system after full lithiation is only 3%, rivals that of the LIB systems. Besides, such design could also provide a kinetic barrier for Li<sub>2</sub>S<sub>y</sub> dissolution. All our findings show that Mn-HAB-CP could be a potentially promising Li-S cathode material, and offer a new computational framework to investigate the Li-S battery and other processed with solvent effects.

## Supporting information

The details of Gibbs free formation energies, experiment voltage vs calculated voltage, the process of the in-house global minimum structure search code, the induced polarization charges of  $\text{Li}_2\text{S}_y$  ( $4 \leq y \leq 8$ ), and the side views of optimized stable structure of  $\text{Li}_x\text{S}_y$  adsorbed on Mn-HAB-CP can be found in the supporting information.

## Acknowledgment

This work was supported by the Assistant Secretary for Energy Efficiency and Renewal Energy of the U. S. Department of Energy under the Battery Materials Research (BMR) program. The theoretical work in this research used the resources of the National Energy Research Scientific Computing Center (NERSC) that is supported by the Office of Science of the U. S. Department of Energy.

## Reference

- [1] J. B. Goodenough, K.-S. Park, *J. Am. Chem. Soc.* **2013**, 135, 1167.
- [2] Y. Liu, G. Zhou, K. Liu, Y. Cui, *Acc. Chem. Res.* **2017**, 50, 2895.
- [3] P. G. Bruce, S. A. Freunberger, L. J. Hardwick, J.-M. Tarascon, *Nat. Mater.* **2011**, 11, 19.
- [4] a) A. Manthiram, Y. Fu, Y.-S. Su, *Acc. of Chem. Res.* **2013**, 46, 1125; b) R. Xu, J. Lu, K. Amine, *Adv. Energy Mater.* **2015**, 5, 1500408.
- [5] N. Imanishi, O. Yamamoto, *Mater. Today* **2014**, 17, 24.
- [6] a) Z. Sun, J. Zhang, L. Yin, G. Hu, R. Fang, H.-M. Cheng, F. Li, *Nat. Commun.* **2017**, 8, 14627; b) L. Zhang, D. Sun, J. Feng, E. J. Cairns, J. Guo, *Nano Letters* **2017**, 17, 5084; c) A. Manthiram, Y. Fu, S.-H. Chung, C. Zu, Y.-S. Su, *Chem. Rev.* **2014**, 114, 11751.
- [7] a) X. Ji, K. T. Lee, L. F. Nazar, *Nat. Mater.* **2009**, 8, 500; b) Y. Li, K. K. Fu, C. Chen, W. Luo, T. Gao, S. Xu, J. Dai, G. Pastel, Y. Wang, B. Liu, J. Song, Y. Chen, C. Yang, L. Hu, *ACS Nano* **2017**, 11, 4801; c) H. Ting-Zheng, C. Xiang, P. Hong-Jie, H. Jia-Qi, L. Bo-Quan, Z. Qiang, L. Bo, *Small* **2016**, 12, 3283.
- [8] S. Zheng, Y. Wen, Y. Zhu, Z. Han, J. Wang, J. Yang, C. Wang, *Adv. Energy Mater.* **2014**, 4, 1400482.
- [9] G. Zhou, J. Sun, Y. Jin, W. Chen, C. Zu, R. Zhang, Y. Qiu, J. Zhao, D. Zhuo, Y. Liu, X. Tao, W. Liu, K. Yan, H. R. Lee, Y. Cui, *Adv. Mater.* **2017**, 29, 1603366.
- [10] Y. Li, K. Yan, H.-W. Lee, Z. Lu, N. Liu, Y. Cui, *Nat. Energy* **2016**, 1, 15029.
- [11] a) H. Wang, T. Zhou, D. Li, H. Gao, G. Gao, A. Du, H. Liu, Z. Guo, *ACS Appl. Mater. Interfaces* **2017**, 9, 4320; b) Z. Yuan, H.-J. Peng, T.-Z. Hou, J.-Q. Huang, C.-M. Chen, D.-W. Wang, X.-B. Cheng, F. Wei, Q. Zhang, *Nano Lett.* **2016**, 16, 519.
- [12] Q. Pang, D. Kundu, L. F. Nazar, *Mater. Horiz.* **2016**, 3, 130.
- [13] R. Demir-Cakan, M. Morcrette, F. Nouar, C. Davoisne, T. Devic, D. Gonbeau, R. Dominko, C. Serre, G. Férey, J.-M. Tarascon, *J. Am. Chem. Soc.* **2011**, 133, 16154.
- [14] L. Wang, Y. Han, X. Feng, J. Zhou, P. Qi, B. Wang, *Coord. Chem. Rev.* **2016**, 307, 361.
- [15] N. Lahiri, N. Lotfizadeh, R. Tsuchikawa, V. V. Deshpande, J. Louie, *J. Am. Chem. Soc.* **2017**, 139, 19.
- [16] G. Gao, E. R. Waclawik, A. Du, *J. Catal.* **2017**, 352, 579.

- [17] D. Feng, T. Lei, M. R. Lukatskaya, J. Park, Z. Huang, M. Lee, L. Shaw, S. Chen, A. A. Yakovenko, A. Kulkarni, J. Xiao, K. Fredrickson, J. B. Tok, X. Zou, Y. Cui, Z. Bao, *Nat. Energy* **2018**, 3, 30.
- [18] a) F. Li, J. Zhao, *Phys. Chem. Chem. Phys.* **2018**, 20, 4005; b) F. Li, J. Zhao, *ACS Appl. Mater. Interfaces* **2017**, 9, 42836; c) L.-C. Yin, J. Liang, G.-M. Zhou, F. Li, R. Saito, H.-M. Cheng, *Nano Energy* **2016**, 25, 203.
- [19] T. A. Pham, M. Govoni, R. Seidel, S. E. Bradforth, E. Schwegler, G. Galli, *Sci. Adv.* **2017**, 3.
- [20] G. Zhou, H. Tian, Y. Jin, X. Tao, B. Liu, R. Zhang, Z. W. Seh, D. Zhuo, Y. Liu, J. Sun, J. Zhao, C. Zu, D. S. Wu, Q. Zhang, Y. Cui, *Proc. Natl. Acad. Sci.* **2017**, 114, 840.
- [21] a) W. Jia, Z. Cao, L. Wang, J. Fu, X. Chi, W. Gao, L.-W. Wang, *Comput. Phys. Commun.* **2013**, 184, 9; b) W. Jia, J. Fu, Z. Cao, L. Wang, X. Chi, W. Gao, L.-W. Wang, *J. Comput. Phys.* **2013**, 251, 102.
- [22] J. P. Perdew, K. Burke, M. Ernzerhof, *Phys. Rev. Lett.* **1996**, 77, 3865.
- [23] J. P. Perdew, M. Ernzerhof, K. Burke, *J. Chem. Phys.* **1996**, 105, 9982.
- [24] S. Grimme, *J. Comput. Chem.* **2006**, 27, 1787.
- [25] S. L. Dudarev, G. A. Botton, S. Y. Savrasov, C. J. Humphreys, A. P. Sutton, *Phys. Rev. B* **1998**, 57, 1505.
- [26] J. Tomasi, B. Mennucci, R. Cammi, *Chem. Rev.* **2005**, 105, 2999.
- [27] C. Dupont, O. Andreussi, N. Marzari, *J. Chem. Phys.* **2013**, 139, 214110.
- [28] R. E. Skyner, J. L. McDonagh, C. R. Groom, T. van Mourik, J. B. O. Mitchell, *Phys. Chem. Chem. Phys.* **2015**, 17, 6174.
- [29] X. Chen, H.-J. Peng, R. Zhang, T.-Z. Hou, J.-Q. Huang, B. Li, Q. Zhang, *ACS Energy Lett.* **2017**, 2, 795.
- [30] a) D. Ghosh, A. Roy, R. Seidel, B. Winter, S. Bradforth, A. I. Krylov, *J. Phys. Chem. B* **2012**, 116, 7269; b) R. S. Assary, L. A. Curtiss, J. S. Moore, *J. Phys. Chem. C* **2014**, 118, 11545.
- [31] C. Barchasz, F. Molton, C. Duboc, J.-C. Leprêtre, S. Patoux, F. Alloin, *Anal. Chem.* **2012**, 84, 3973.
- [32] a) J. Wu, L.-W. Wang, *J. Mater. Chem. A* **2018**, 6, 2984; b) N. N. Rajput, V. Murugesan, Y. Shin, K. S. Han, K. C. Lau, J. Chen, J. Liu, L. A. Curtiss, K. T. Mueller, K. A. Persson, *Chem. Mater.* **2017**, 29, 3375.
- [33] G. Yang, S. Shi, J. Yang, Y. Ma, *J. Mater. Chem. A* **2015**, 3, 8865.
- [34] B. Wang, S. M. Alhassan, S. T. Pantelides, *Phys. Rev. Appl.* **2014**, 2, 034004.
- [35] Z. W. Seh, J. H. Yu, W. Li, P.-C. Hsu, H. Wang, Y. Sun, H. Yao, Q. Zhang, Y. Cui, *Nat. Commun.* **2014**, 5, 5017.
- [36] S. Darby, T. V. Mortimer-Jones, R. L. Johnston, C. Roberts, *J. Chem. Phys.* **2002**, 116, 1536.
- [37] Y. Yang, M. T. McDowell, A. Jackson, J. J. Cha, S. S. Hong, Y. Cui, *Nano Lett.* **2010**, 10, 1486.



TOC

